

Electronic Supplementary Information

Supramolecular squares of Sn(IV)porphyrins with Re(I)-corners for the fabrication of self-assembled nanostructures performing photocatalytic degradation of Eriochrome Black T dye

Nirmal Kumar Shee and Hee-Joon Kim*

*Department of Chemistry and Bioscience, Kumoh National Institute of Technology
61 Daehak-ro, Gumi 39177, Republic of Korea*

List of contents:

Fig. S1 ^1H -NMR spectrum of *trans*-[5,15-bis(4-pyridyl)-10,20-bis(4-*tert*-butylphenyl)porphyrin] H_2P^2 in CDCl_3 .

Fig. S2 ^1H -NMR spectrum of *trans*-[5,15-bis(4-pyridyl)-10,20-bis(4-*tert*-butylphenyl)porphyrinato]tin(IV) SnP^2 in CDCl_3 .

Fig. S3 ^1H -NMR spectrum of **1** in CDCl_3 .

Fig. S4 ^1H -NMR spectrum of **2** in CDCl_3 .

Fig. S5 Electrospray ionization mass (ESI-MS) spectrum of SnP^2 .

Fig. S6 ESI-MS spectrum of **1**.

Fig. S7 ESI-MS spectrum of **2**.

Fig. S8 Thermogravimetric analysis (TGA) curves of **1** and **2**.

Fig. S9 Powder X-ray diffraction (PXRD) patterns of **1** and **2**.

Fig. S10 Particle size determination by dynamic light scattering (DLS) for **1** and **2** in toluene.

Fig. S11 Field emission scanning electron microscopy (FE-SEM) images for SnP^1 (a) and SnP^2 (b).

Fig. S12 Adsorption and desorption isotherms of N_2 for **1** and **2** at 77 K.

Fig. S13 Adsorption of Eriochrome Black T (EBT) dye on **1** and **2**.

Fig. S14 Time-dependent absorption spectra of EBT dye in the presence of **2** under visible-light irradiation.

Fig. S15 Kinetics of the photocatalytic degradation of EBT dye under visible-light irradiation by photocatalysts **1** and **2**.

Fig. S16 Typical catalytic cycle (up to 10 consecutive cycles) of photocatalyst **2** for the degradation of EBT dye.

Table S1. Pseudo-first-order degradation rate constant of EBT dye for each cycle.

Fig. S17 Typical FE-SEM images of photocatalysts **1** (a) and **2** (b) after the degradation of EBT dye (10 consecutive cycles).

Fig. S18 Effect of temperature on the degradation of EBT dye by **2**.

Fig. S19 Effect of pH of the EBT dye solution on the photodegradation by **2**.

Fig. S20 Effect of EBT dye concentration on the photodegradation by **2** (20 mg) within 90 min of visible-light irradiation.

Fig. S21 Effect of various scavengers on the degradation of EBT dye in the presence of **2** under visible-light irradiation ($[\text{Na}_2\text{-EDTA}]_0 = [\text{p-BQ}]_0 = [\text{tBuOH}]_0 = 5\text{mM}$, pH 7.0, T = 298 K). SnP^1 and SnP^2 were used as catalysts for comparison.

Fig. S22 Photocatalytic activities of **2** at different wavelengths for the degradation of EBT dye.

Fig. S23 Negative ion mode ESI-MS spectrum of the reaction mixture of EBT dye in the presence of **2** after 45 min of visible-light irradiation.

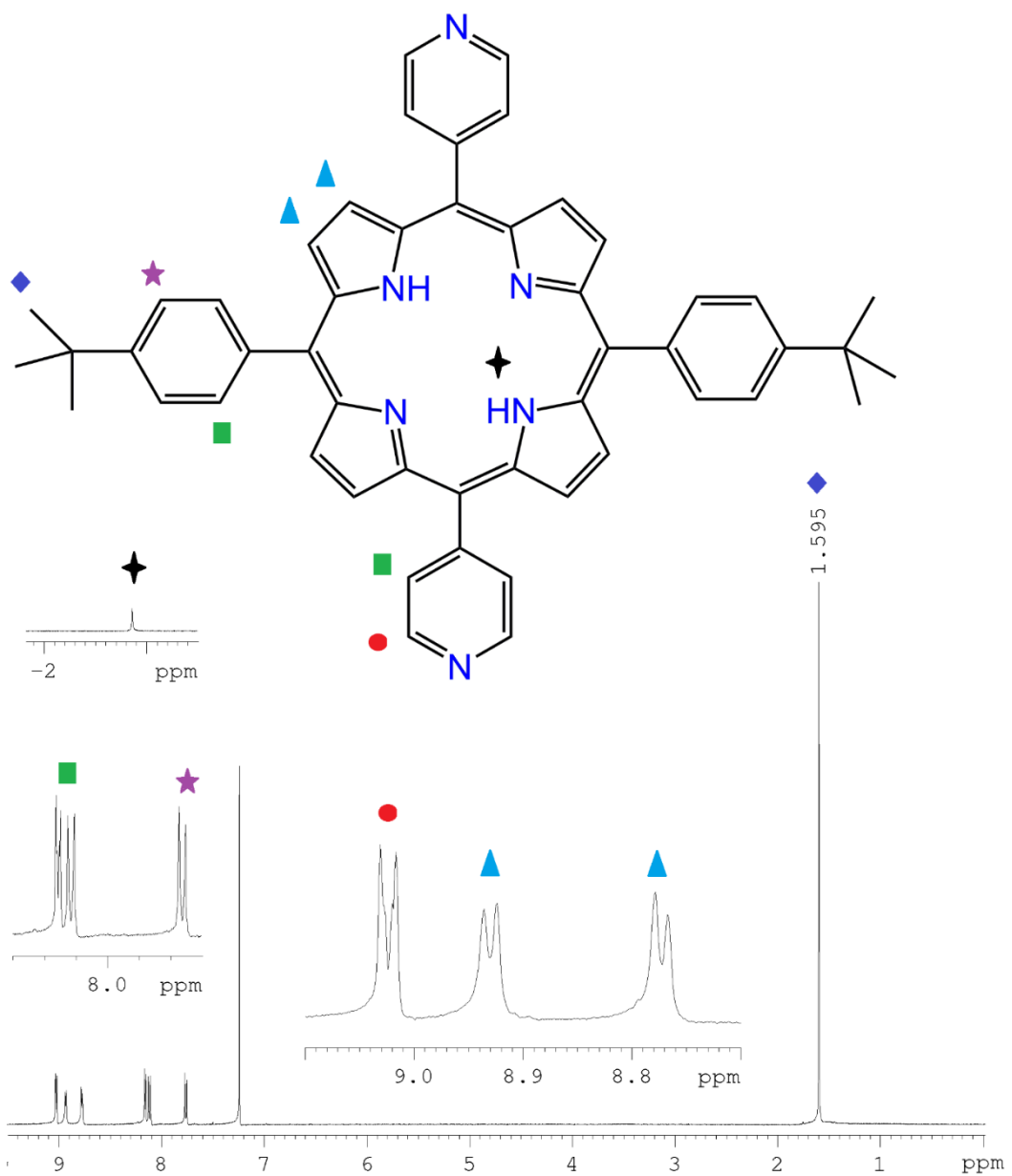


Fig. S1 ¹H-NMR spectrum of *trans*-[5,15-bis(4-pyridyl)-10,20-bis(4-*tert*-butylphenyl)porphyrin] H₂P² in CDCl₃.

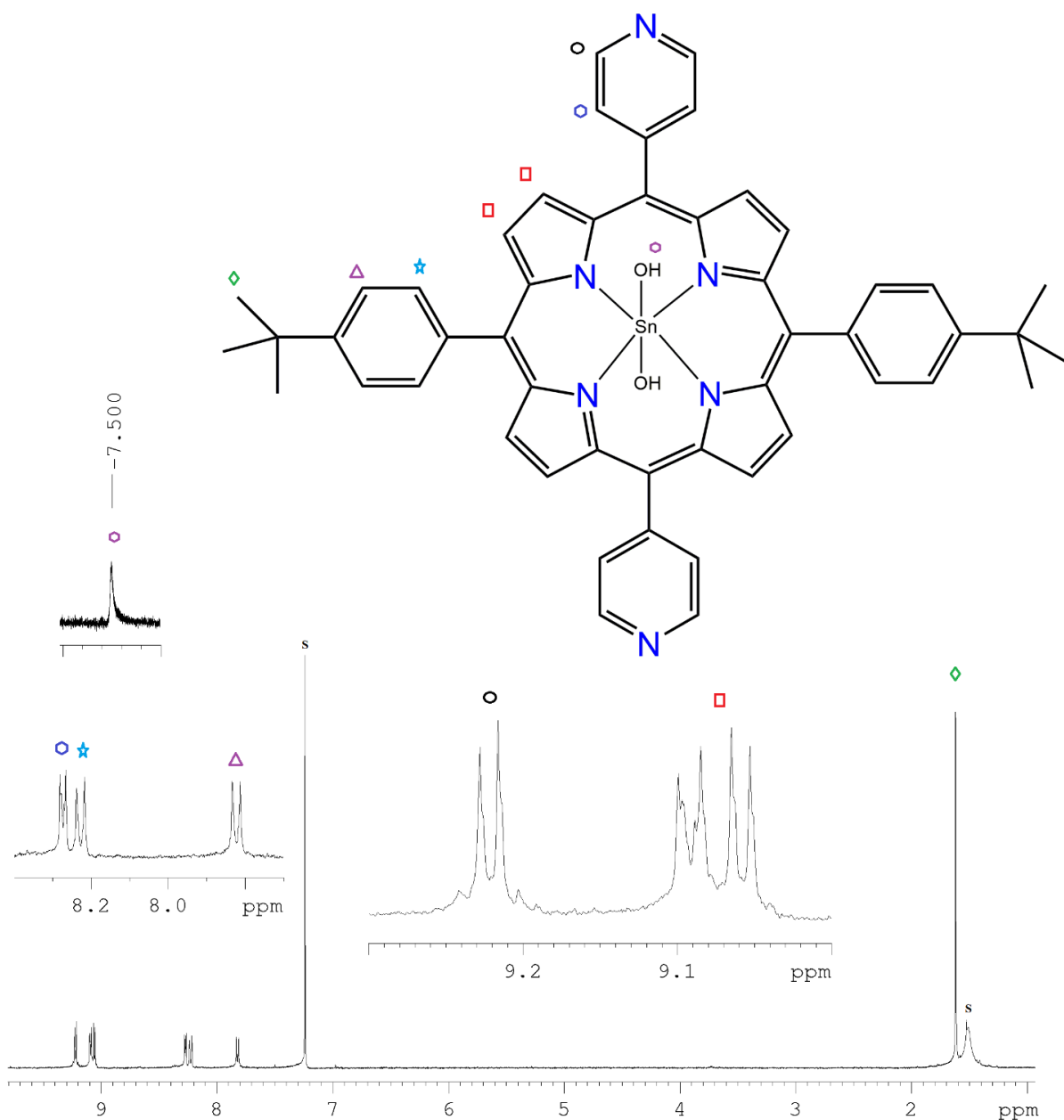


Fig. S2 ¹H-NMR spectrum of *trans*-[5,15-bis(4-pyridyl)-10,20-bis(4-*tert*-butylphenyl)porphyrinato]tin(IV) **SnP²** in CDCl₃.

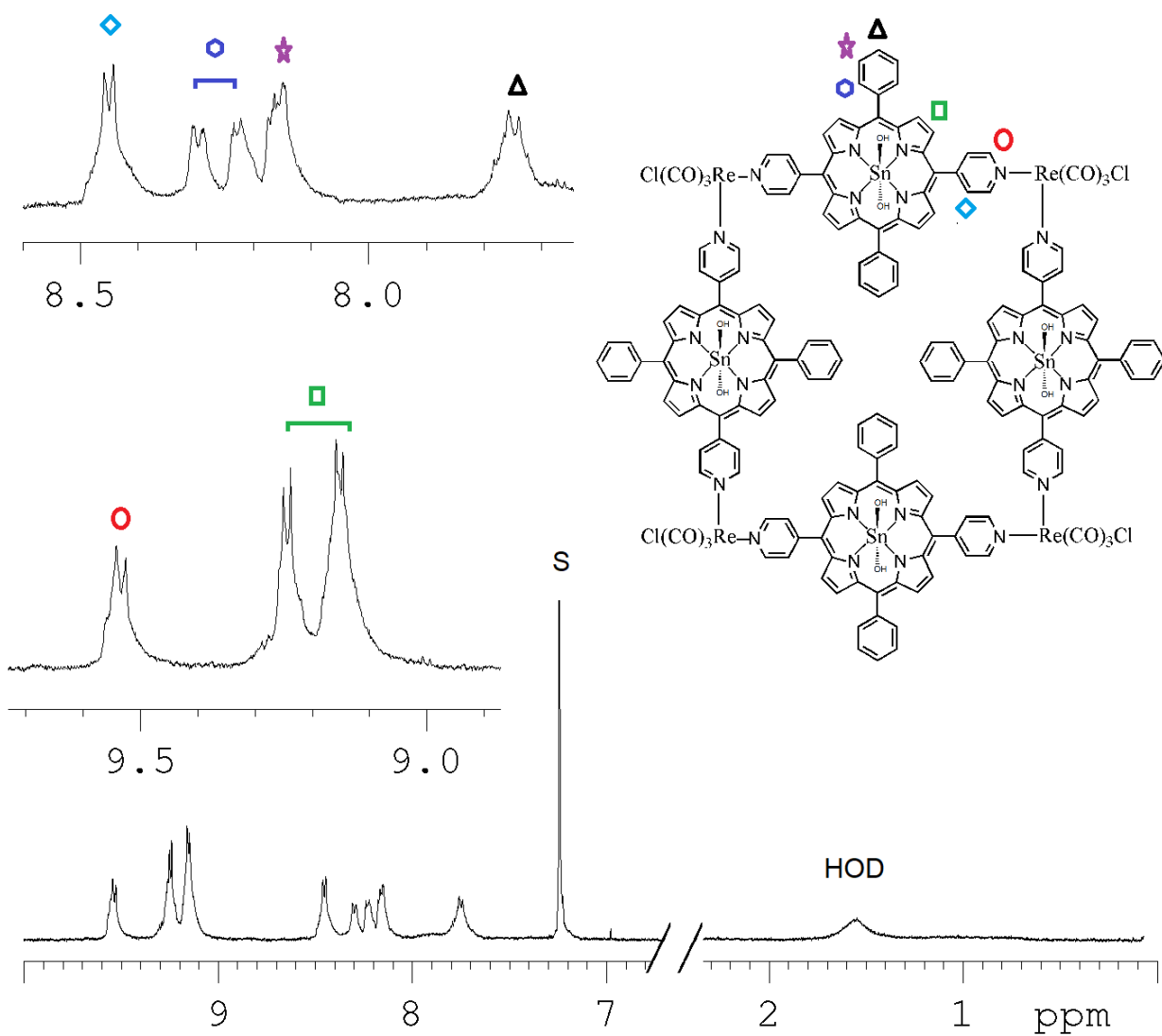


Fig. S3 ^1H -NMR spectrum of **1** in CDCl_3 .

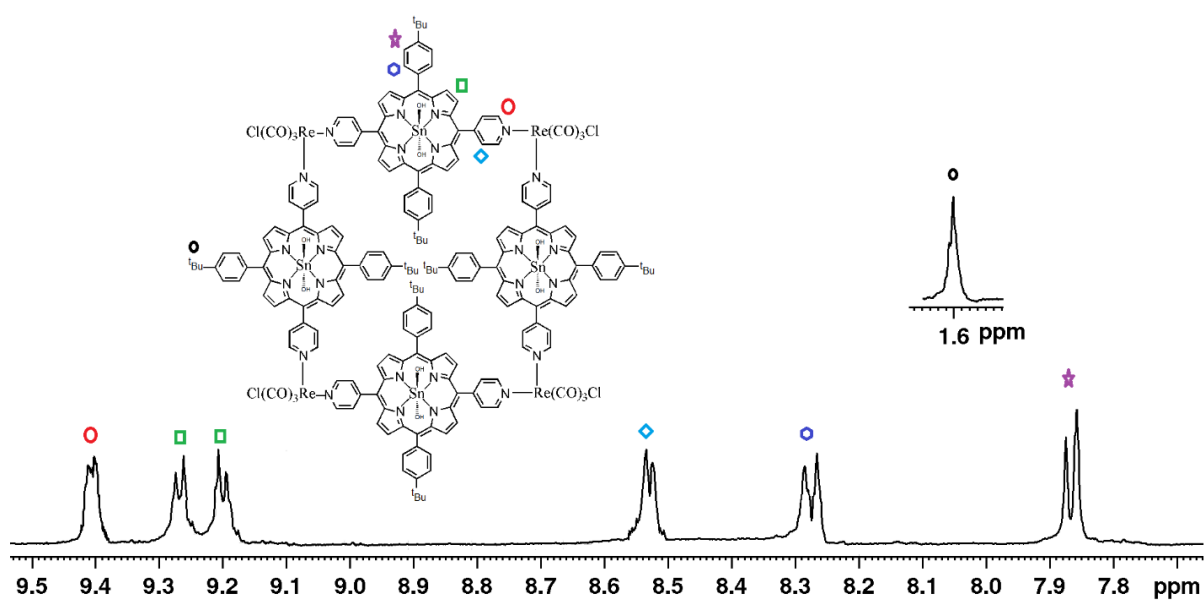


Fig. S4 ^1H -NMR spectrum of **2** in CDCl_3 .

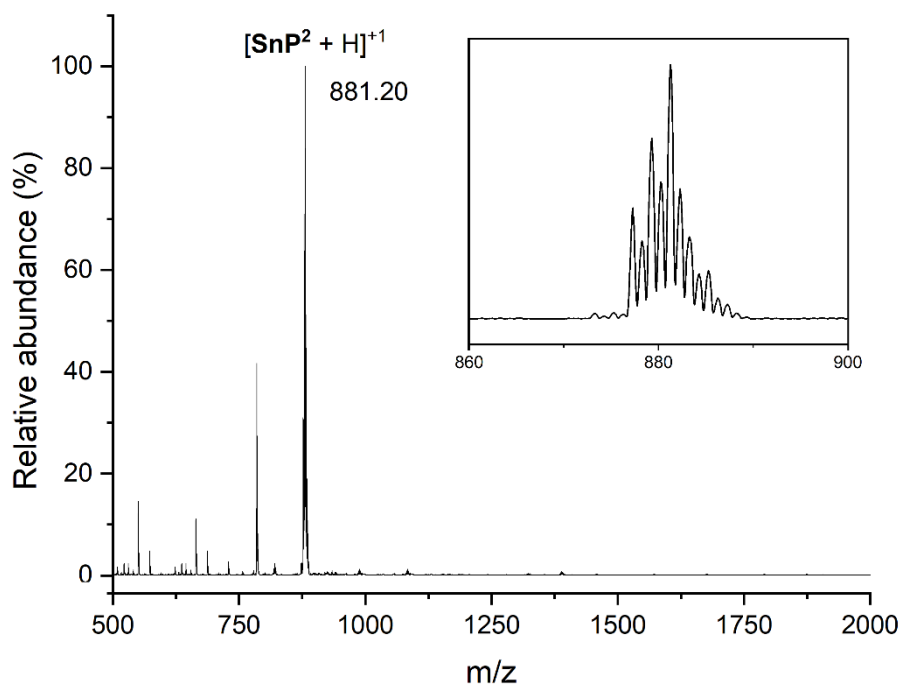


Fig. S5 Electrospray ionization mass (ESI-MS) spectrum of SnP^2 .

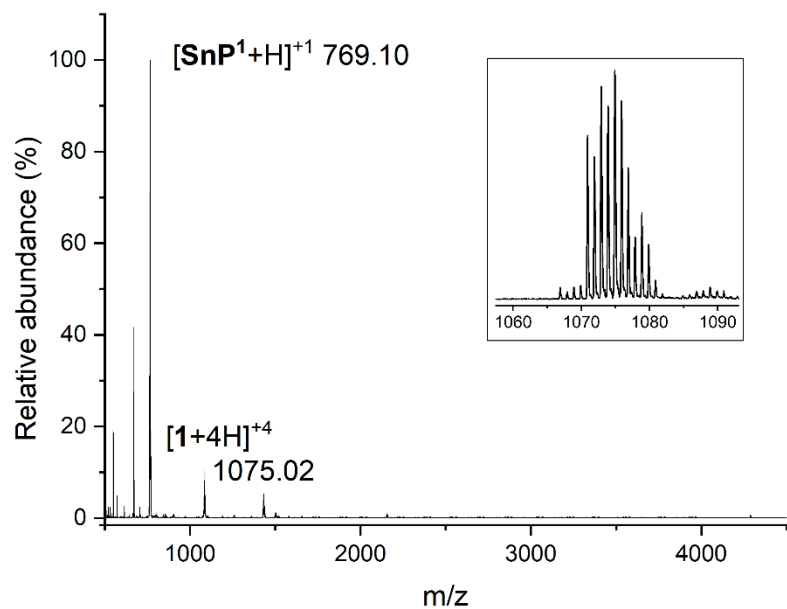


Fig. S6 ESI-MS spectrum of **1**.

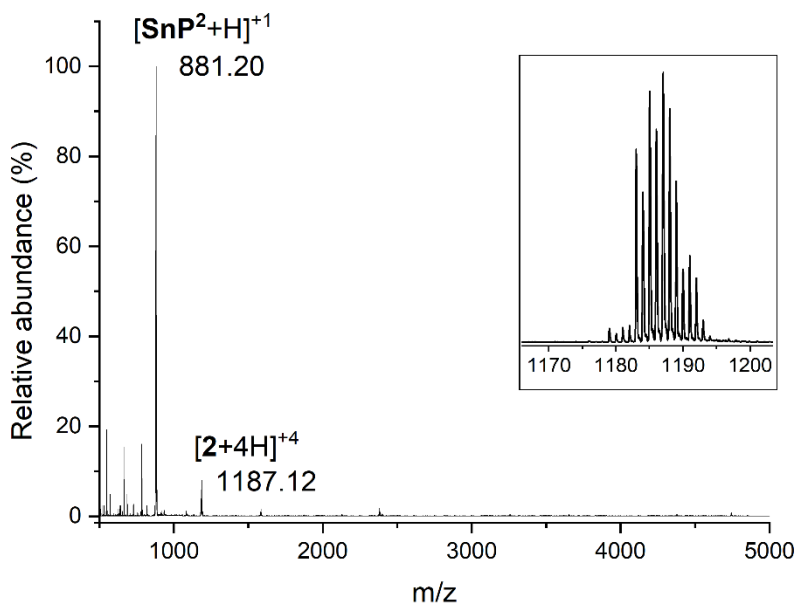


Fig. S7 ESI-MS spectrum of **2**.

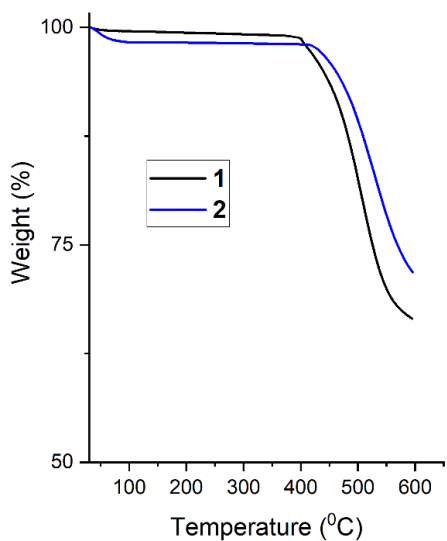


Fig. S8 Thermogravimetric analysis (TGA) curves of **1** and **2**.

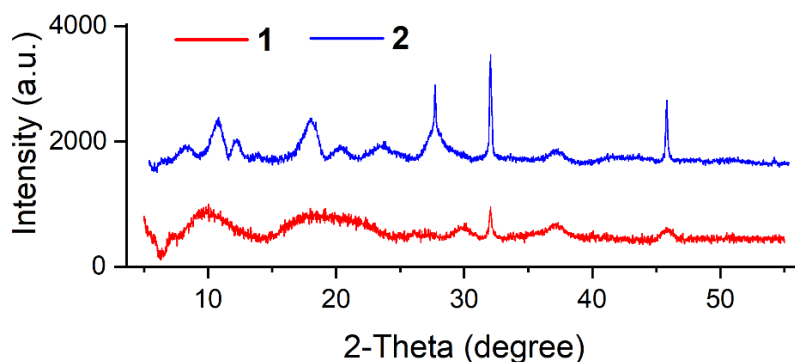


Fig. S9 Powder X-ray diffraction (PXRD) patterns of **1** and **2**.

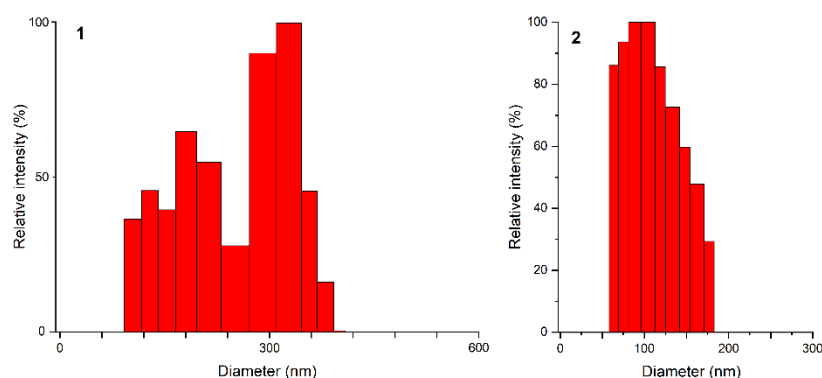


Fig. S10 Particle size determination by dynamic light scattering (DLS) for **1** and **2** in toluene.

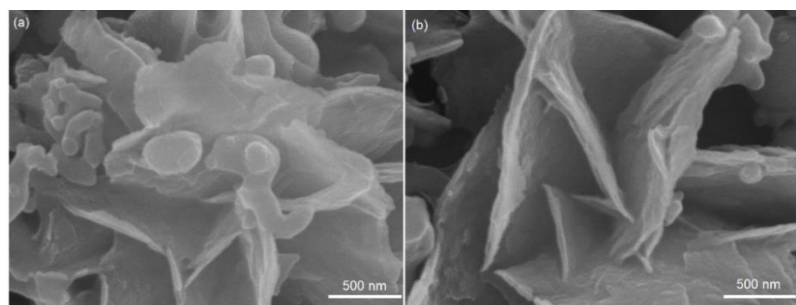


Fig. S11 Field emission scanning electron microscopy (FE-SEM) images for SnP¹ (a) and SnP² (b).

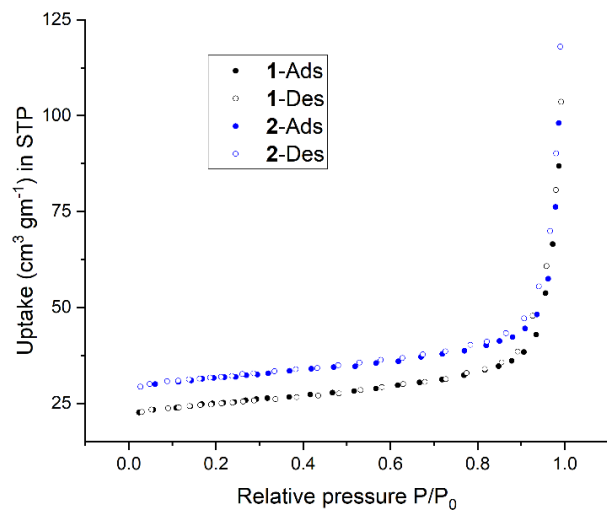


Fig. S12 Adsorption and desorption isotherms of N_2 for **1** and **2** at 77 K.

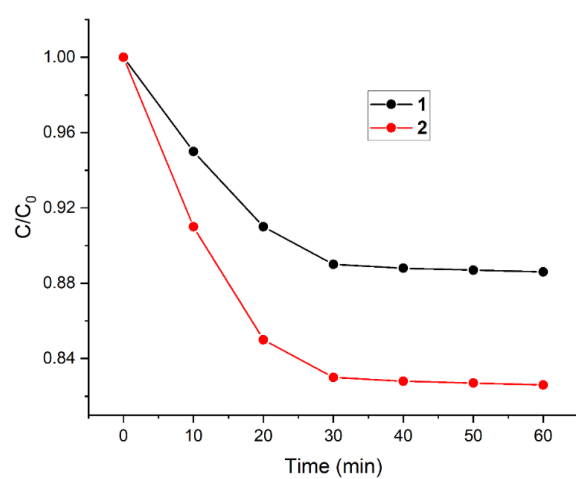


Fig. S13 Adsorption of Eriochrome Black T (EBT) dye on **1** and **2**.

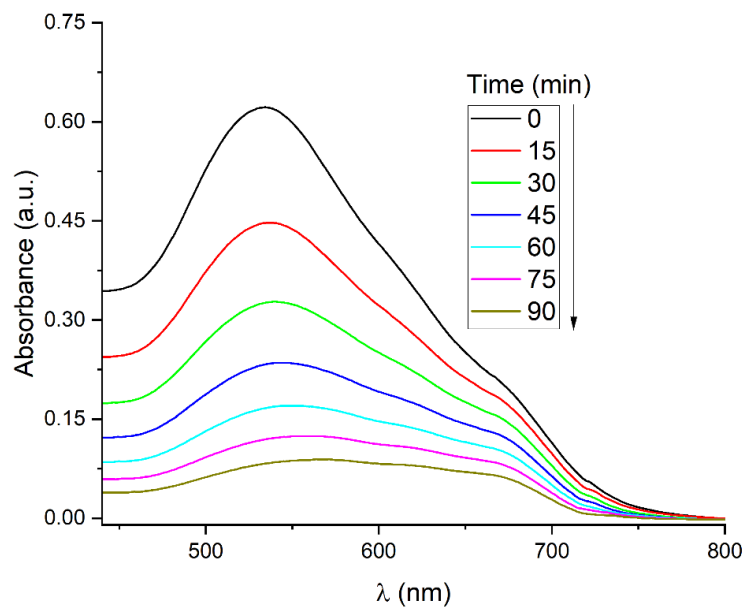


Fig. S14 Time-dependent absorption spectra of EBT dye in the presence of **2** under visible-light irradiation.

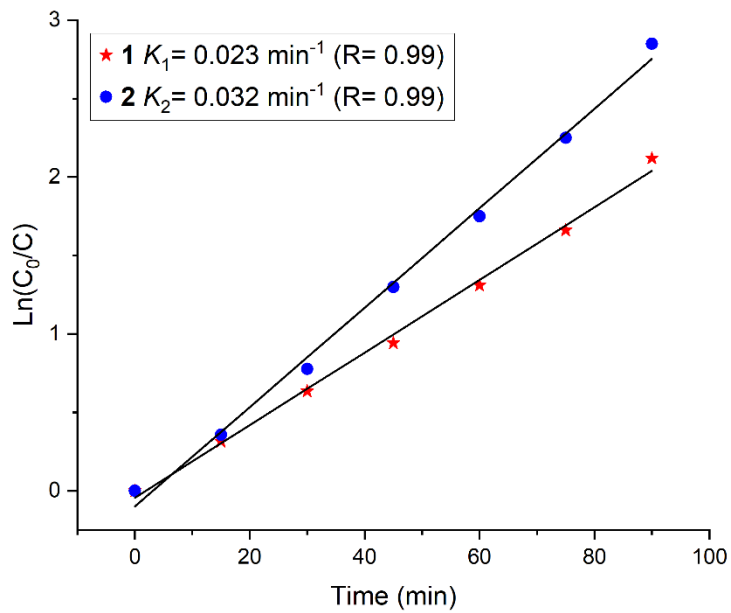


Fig. S15 Kinetics of the photocatalytic degradation of EBT dye under visible-light irradiation by photocatalysts **1** and **2**.

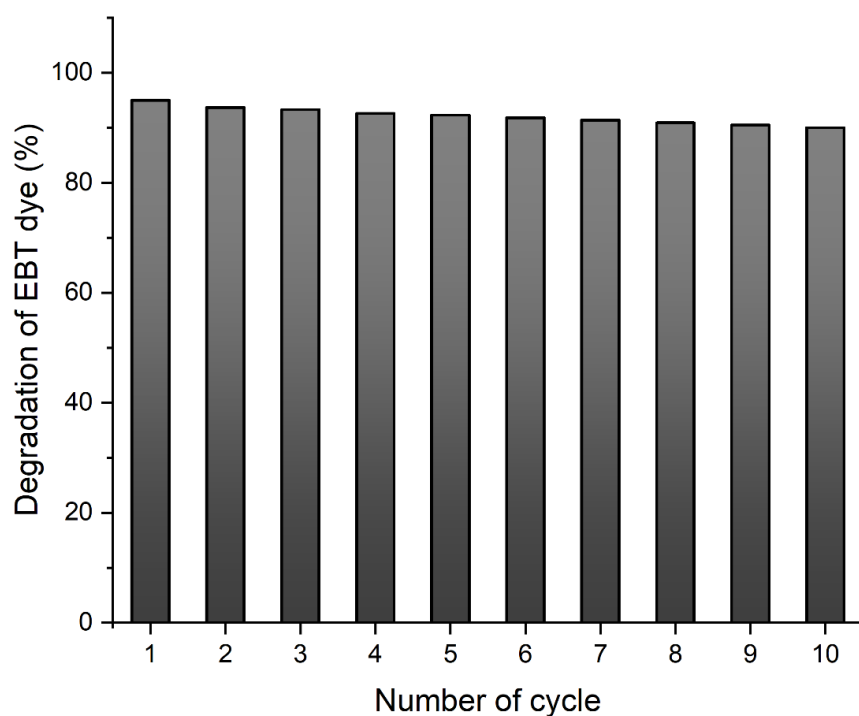


Fig. S16 Typical catalytic cycle (up to consecutive 10 cycles) of photocatalyst **2** for the degradation of EBT dye.

Table S1. Pseudo-first-order degradation rate constant of EBT dye for each cycle.

| Number of cycle | Rate constant k (min^{-1}) |
|-----------------|---|
| 1 | 0.0320 |
| 2 | 0.0317 |
| 3 | 0.0313 |
| 4 | 0.0309 |
| 5 | 0.0305 |
| 6 | 0.0301 |
| 7 | 0.0298 |
| 8 | 0.0295 |
| 9 | 0.0292 |
| 10 | 0.0290 |

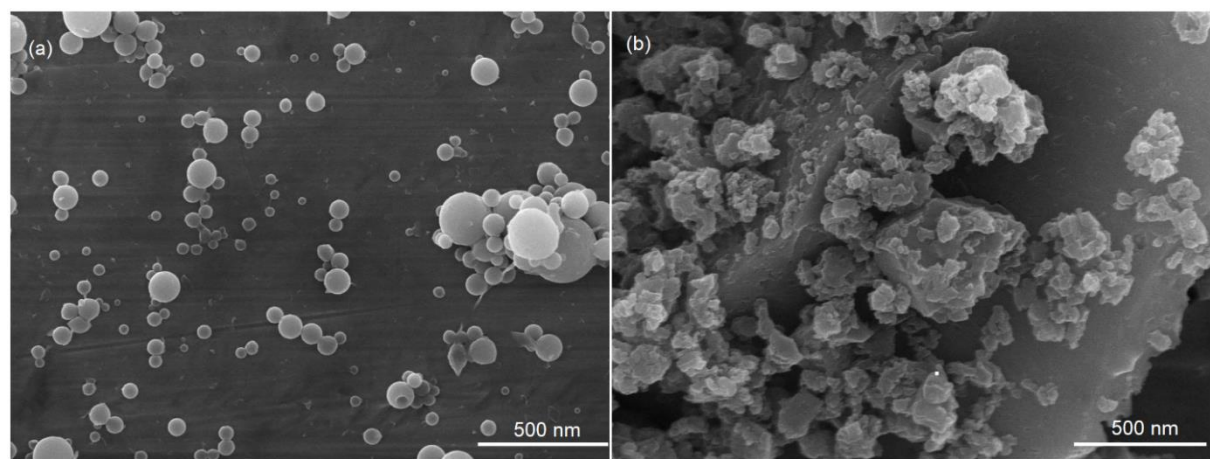


Fig. S17 Typical FE-SEM images of photocatalysts **1** (a), and **2** (b) after the degradation of EBT dye (consecutive 10 cycles).

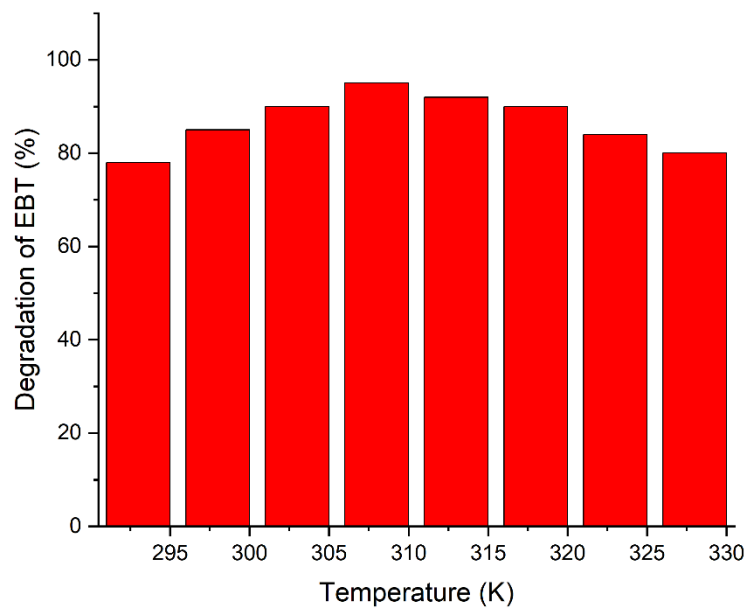


Fig. S18 Effect of temperature on the degradation of EBT dye by **2**.

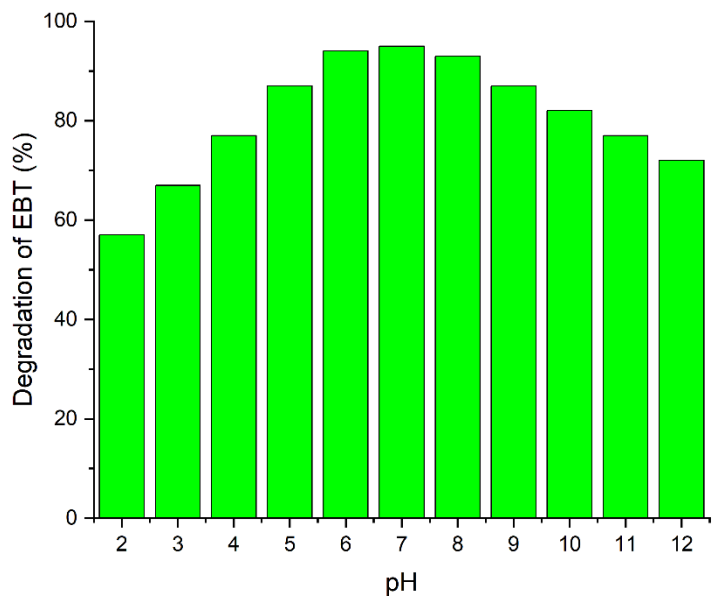


Fig. S19 Effect of pH of the EBT dye solution on the photodegradation by **2**.

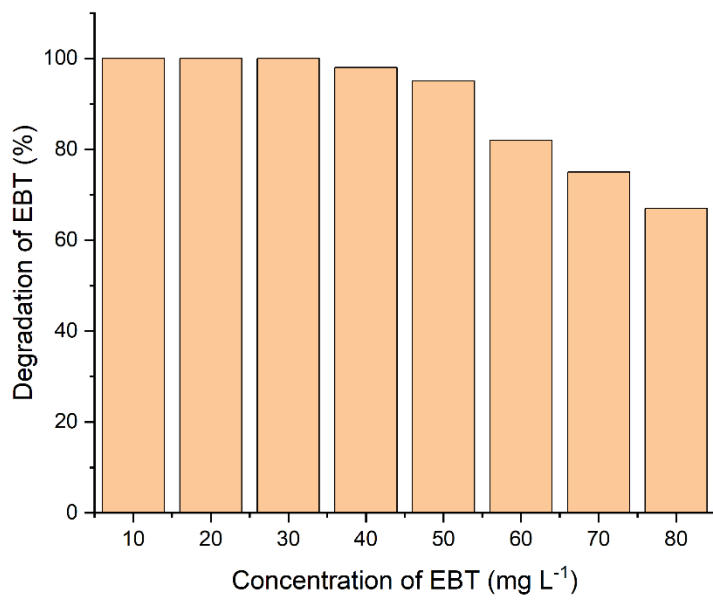


Fig. S20 Effect of EBT dye concentration on the photodegradation by **2** (20 mg) within 90 min of visible-light irradiation.

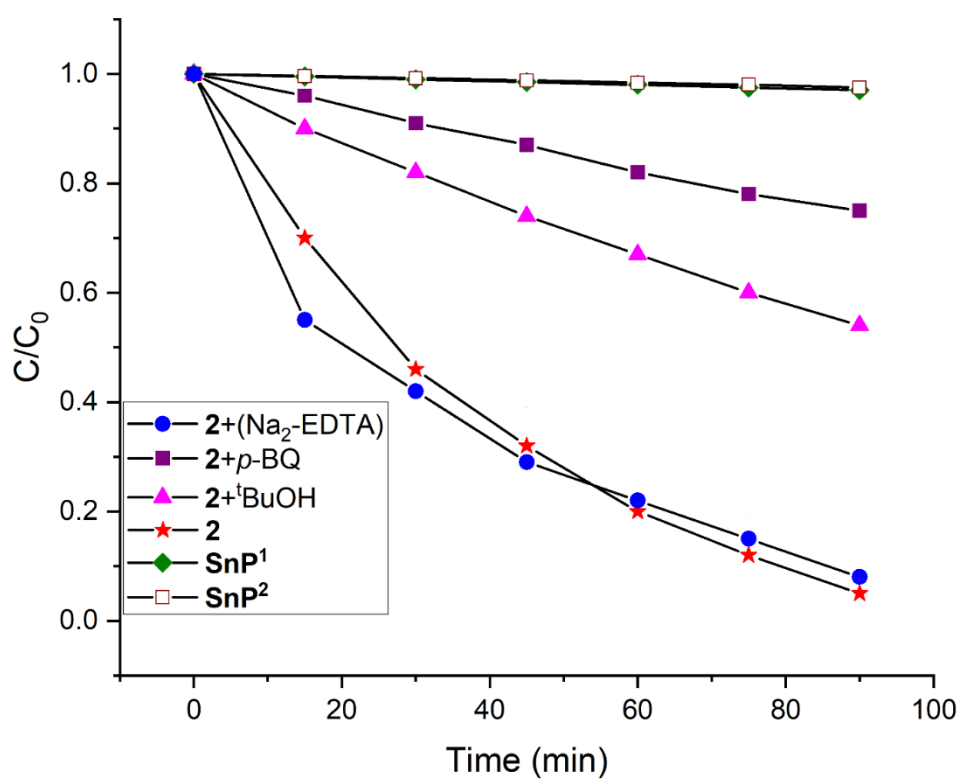


Fig. S21 Effect of various scavengers on the degradation of EBT dye in the presence of **2** under visible-light irradiation ($[\text{Na}_2\text{-EDTA}]_0 = [p\text{-BQ}]_0 = [\text{tBuOH}]_0 = 5\text{mM}$, pH 7.0, T = 298 K). SnP^1 and SnP^2 were used as catalysts for comparison.

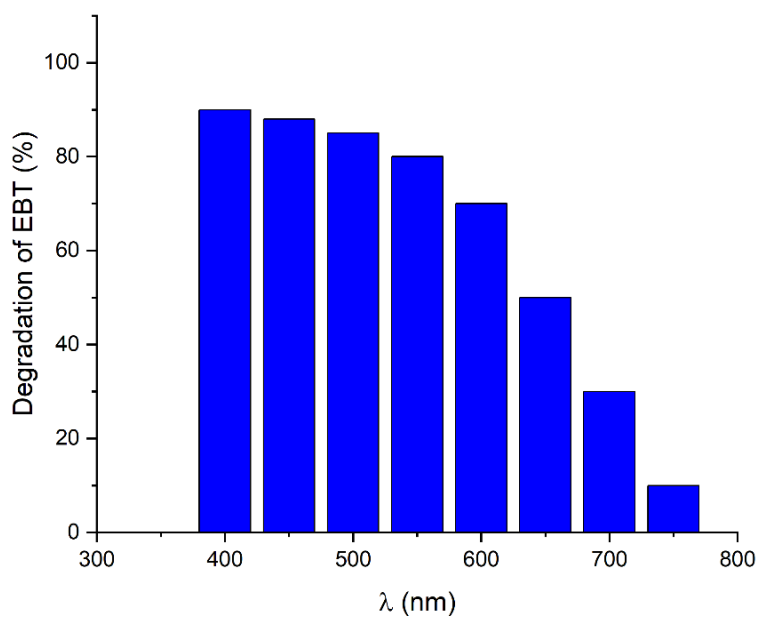


Fig. S22 Photocatalytic activities of **2** at different wavelengths for the degradation of EBT dye.

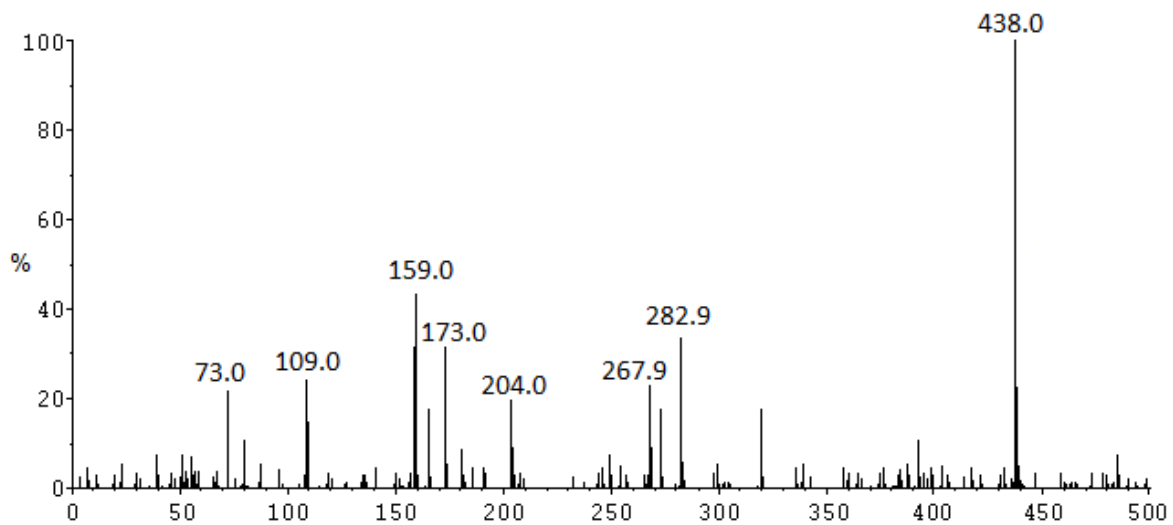


Fig. S23 Negative ion mode ESI-MS spectrum of the reaction mixture of EBT dye in the presence of **2** after 45 min of visible-light irradiation.
